Asian Journal of Chemistry; Vol. 36, No. 12 (2024), 2939-2945

ASIAN JOURNAL OF CHEMISTRY

https://doi.org/10.14233/ajchem.2024.32759

Amorphous Zirconium-Zinc Bimetallic Metal Organic Framework based Fluorescent Sensor for Sensing of Ceftriaxone, Metronidazole and Ornidazole Antibiotics

JAYASREE KOMARA, JAYA PRASANTHI KARUMURI*, RAVIKANTH TANDRA and SANTHOSH THOTA

Department of Chemistry, AU College of Science and Technology, Andhra University, Visakhapatnam-530003, India

*Corresponding author: E-mail: dr.kjprasanthi@andhrauniversity.edu.in

Received: 23 September 2024; *Accepted*: 15 November 2024; *Published online*: 30 November 2024; AJC-21838

It is essential to have both sensitive and selective antibiotic sensor, as the overuse of antibiotics has escalated in the last few years, endangering both human health and the environment. This work produced a hydrostable amorphous bimetallic metal organic framework (Zr-Zn-EDTA), which is employed as a fluorescence sensor using a solvothermal approach. Zr-Zn-EDTA bimetallic metal organic framework effectively quenches ceftriaxone, metronidazole and ornidazole among the five antibiotics, with low detection limits (LOD) 4.9×10^{-7} M for ceftriaxone, 5.4×10^{-7} M for metronidazole and 6.05×10^{-7} M for ornidazole, respectively. Moreover, Zr-Zn-EDTA exhibits good selectivity and recyclability for the detection of antibiotics including metronidazole, ornidazole and ceftriaxone. Specifically, a comprehensive analysis of the quenching mechanism has been shown, which might offer a clear comprehension for the identification of the ensuing antibiotics.

Keywords: Zirconium, Zinc, Ethylene diaminetetraacetate, Sensor, Metal organic framework, Bimetallic MOFs, Antibiotics.

INTRODUCTION

One of the most intriguing families of porous materials to be found in the last several decades are metal organic frameworks (MOFs). In order to develop intriguing polymeric frameworks with a greater surface area and the benefit of pore size modification, MOFs are adaptable materials made by organic molecules (linkers) linked to metal ions or clusters. MOF materials are used in medication delivery, gas storage, gas separation, heterogeneous catalysis, magnetic refrigeration, sensing and energy storage because of their porosity and tuneable textural features [1]. While amorphous MOFs (aMOFs) have just lately begun to surface as well-characterized examples, a small but growing number of non-crystalline MOFs are attracting scientific attention. For the sake of simplicity, an amorphous MOF is defined as a network of inorganic nodes, such as metal ions or clusters, connected by organic ligands, which are often nitrogen based or carboxylate-based functional groups. The absence of Bragg peaks in their X-ray or neutron diffraction patterns indicates that there is no long-range order in the structure, which is crucial (and clearly distinguishes them from crystalline MOFs) [2]. Although the domain is mostly unexplored, amorphous MOFs provide many interesting potentials for practical use, either as novel functional materials themselves or enabling other processes.

AmorphousMOFs have been shown to hold promise in a number of areas, including medicine delivery [3], irreversible hazardous substance removal [4], supercapacitors [5] and catalysis [6]. The incorporation of secondary metal ions into framework centers for the fabrication of bimetallic metal-organic frameworks has been proposed as a method to improve their electrical, luminescent and catalytic properties. These MOFs including bimetallic MOFs have higher structural stability and performance, because they incorporate two distinct metal ions into one structure. Second metal ions can partially replace inorganic centers or secondary-building units (SBUs) inside the framework, allowing the bimetallic system to show synergistic effects [7]. Bimetallic metal-organic frameworks can be synthesized through various techniques, including direct synthesis, template synthesis, post-synthetic modification, seed-induced growth, and post-synthetic exchange.

Due to the widespread belief that people should take responsibility for the environment and consequently, safeguard ecosystems to the best of their abilities, the issue of pollution brought on by industrial expansion is currently quite popular. There have been some compounds in the environment in recent

years for which there are no strict rules in place. Together, these substances are known as emerging contaminants (ECs), which are substances of many origins and types that may have an adverse effect on the environment and public health. Additives, personal hygiene items, pesticides, flame retardants and pharmaceuticals are some of the contaminants that are becoming more prevalent [8]. The most often used drugs in the previously stated pharmacological group are antibiotics. These medications are discharged into bodies of water by a number of processes, including bodily excretion, animal dung, poultry, hospital medication disposal and wastewater from the companies that manufacture antibiotics [9,10]. Drug resistance in living things has been caused by overuse of antibiotics [11]. Among the most often prescribed antibiotics are ceftriaxone (CFT), metronidazole (MDZ), ornidazole (ODZ), amikacin (AMK) and levofloxacin (LVF). Ceftriaxone (CFT) is used to treat a range of bacterial infections and it is a third-generation cephalosporin that prevents the synthesis of mucopeptide in bacterial cell walls. Due to its potent antibacterial properties, high lactamase tolerance, positive clinical results, low toxicity and minimal allergic reaction, it is frequently utilized in clinical settings. CFT is 100% bioavailable and eliminated by biliary and renal elimination, according to intramuscular injections [12]. Among the nitroimidazole derivatives is metronidazole (MDZ), which has antibacterial and antiprotozoal characteristics. Seizures, genotoxicity, ataxia, irritated stomach mucous, neutropenia, carcinogenicity, encephalopathy, spermatozoid destruction, mutagenicity and haematuria are only a few of the serious adverse effects linked to MDZ. Extended use of MDZ can result in drug resistance, posing a significant risk to human health. However, several commercial enterprises continue to use MDZ illegally as a component in various cosmetic goods due to its high cost-effectiveness and efficacy in treating infections [13]. Ornidazole (ODZ), 5-nitroimidazole derivative, is commonly used to treat a range of illnesses brought on by bacteria, parasites and fungus, including giardiasis, Crohn's disease and infections with Dientamoeba fragilis. Because of their potential to produce cancer and mutations, nitroimidazoles have been linked to health concerns to both people and wildlife, according to a number of studies [14]. An aminoglycoside with a broad spectrum of activity and little bacterial resistance is amikacin (AMK). When treating Gram-negative infections that are resistant to gentamycin, kanamycin and tobramycin, it is frequently administered parenterally [15].

Antibiotics in water resources can lead to a number of issues, including the toxicity of bacteria, algae, fish and crabs, as well as the development of antibiotic resistance in bacteria. The most popular techniques for detecting antibiotics are capillary electrophoresis (CE), ion mobility spectroscopy (IMS), liquid chromatography-tandem mass spectrometry (LC-MS) and high-performance liquid chromatography (HPLC). But these processes are usually complicated, time-consuming and inconvenient. Conversely, the high-sensitivity and recyclable fluorescence sensors are considered to be good choices for antibiotic detection and have several advantages [16]. Numerous Zr-Zn bimetallic MOFs, such as Zr-Zn-BDC [17], Zr-Zn-BTC [18] and others, have been synthesized. In this work, we synthesized a Zr-Zn bimetallic MOF with EDTA as a ligand. To the best of our knowledge, this is the first published work on the bimetallic MOF of zirconium-zinc-ethylenediamine tetraacetate (Zr-Zn-EDTA). The synthesized amorphous Zr-Zn bimetallic MOF is characterized by Fourier transform infrared spectroscopy (FT-IR), powder X-ray diffraction (PXRD), field emission scanning electron microscopy-energy dispersive X-ray spectroscopy (FESEM-EDS), Brunauer-Emmett-Teller (BET), transmission electron microscopy (TEM), X-ray photoelectron spectroscopy (XPS) and thermogravimetric analysis (TGA).

EXPERIMENTAL

All chemicals were used without further purification and purchased from reputed companies like Coastal Chemicals and Sigma-Aldrich Chemicals. Every glasswares were thoroughly cleaned and then rinsed with double-distilled water before being dried in an oven to remove any chance of contamination.

Synthesis of Zr-Zn-EDTA bimetallic MOF (BMOF): Precisely weighed 3 mM of zinc acetate, 3 mM of zirconium oxychloride and 3 mM of disodium salt of ethylenediamine tetra acetic acid using a digital weighing balance. Then, transferred the weighed materials into a 100 mL reagent bottle. The contents of the reagent container should be dissolved in the second stage by adding 20 mL of ethanol. Added 40 mL of DMF to the mixture and then adjusted the pH's solution between 6 to 8 by using 0.1 N NaOH or 0.1 N CH_3COOH. To obtain a clear solution, the contents of the reagent bottle for 90 min using a magnetic stirrer and a hotplate. Put the reagent bottle's contents in the hot air oven and set the temperature to 140 ºC for 24 h. Centrifuge the white precipitate after removing the 100 mL reagent vial from the hot air oven after a full day. To get rid of any contaminants that may have dissolved in water or an organic solvent, wash the residue four or five times with double-distilled water and then four or five times with ethanol. After letting the residue dry overnight at 70 ºC in a hot air oven, crush it into a fine powder.

Characterization: The FT-IR spectra was taken using Bruker Alfa-II, Powder-XRD Measurements were carried out using Bruker D8 advance X-ray diffractometer, TGA was carried out using Hitachi STA 7300 model, FESEM-EDS was taken by Quanta FEG 250, Quantachrome NOVA touch 4 LX instrument was used for BET analysis using nitrogen isotherms at 77 K, JEOL JEM 2100 plus electron microscope was used for the TEM analysis, XPS was done using AXIS SUPRA X-ray photoelectron spectrometer and fluorescence spectra was taken using Horiba FluoroMax 4 spectrofluorometer.

Sensing experiment: A suspension of 5 mg of BMOF sample was aged for 24 h after being sonicated for 40 min in 5 mL of double distilled water. The suspension was transferred to a quartz cuvette cell that was 1 cm diameter after 24 h period. Antibiotic solutions were quenched in different concentrations for each experiment. The quenching efficiency (QE, %) was calculated as follows:

$$\text{Quenching efficiency (QE, \%)} = \frac{I_0 - I}{I_0} \times 100$$

where I_0 = original peak maximum intensity; I = maximum intensity after adding the analyte.

RESULTS AND DISCUSSION

The FT-IR spectrum of synthesized BMOF was obtained in the 4000-400 cm^{-1} region (Fig. 1a). The peak at 744 cm^{-1} represents the Zn–O stretching and bending modes. The asymmetric stretching vibrations of carboxylate are represented by peaks at 1593 and 1652 cm^{-1}, while symmetric vibrations are represented by substantial absorption bands at 1397 and 1448 cm^{-1} [19]. One of Zr-O distinctive vibration peaks was the absorption peak, located at 553 cm^{-1} [17]. The C-N bond in EDTA chelates has been identified as the absorption band at 1070–1100 cm^{-1} [20].

The amorphous nature of the synthesized BMOF is demonstrated by the lack of distinct, sharp peaks in the powder XRD are observed in Fig. 1b. There are three stages of weight reduction, as shown by the thermograms of BMOF in Fig. 1c at temperatures between 30 and 1000 ºC. The loss of ethanol and water in the temperature range of 31 to 88 ºC is attributed for the first weight loss, which was about 18.6%. The second weight loss approximately 12.3% was occured by the DMF solvent evaporating at temperatures between 99 and 204 ºC. The breakdown of organic linkers in BMOF and the subsequent production of ZnO and ZrO_2 as end products in the final black powder residue were the main causes of the third loss, which occurred at temperatures between 216 and 446 ºC and accounted for roughly 66.8% of the total loss.

Morphological studies: Fig. 2a-d FESEM pictures reveal the presence of particles with varying sizes and shapes on a surface which is comparatively homogeneous and amorphous. The EDX spectra in Fig. 3a shows the presence of the zirconium

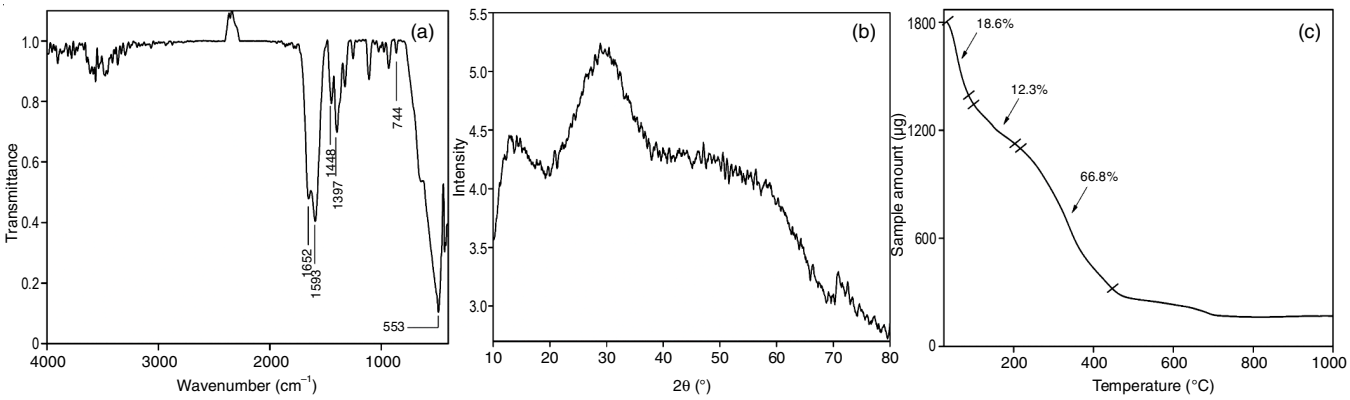

Fig. 1. (a) FT-IR spectra, (b) PXRD spectrum and (c) TGA thermogram of synthesized BMOF

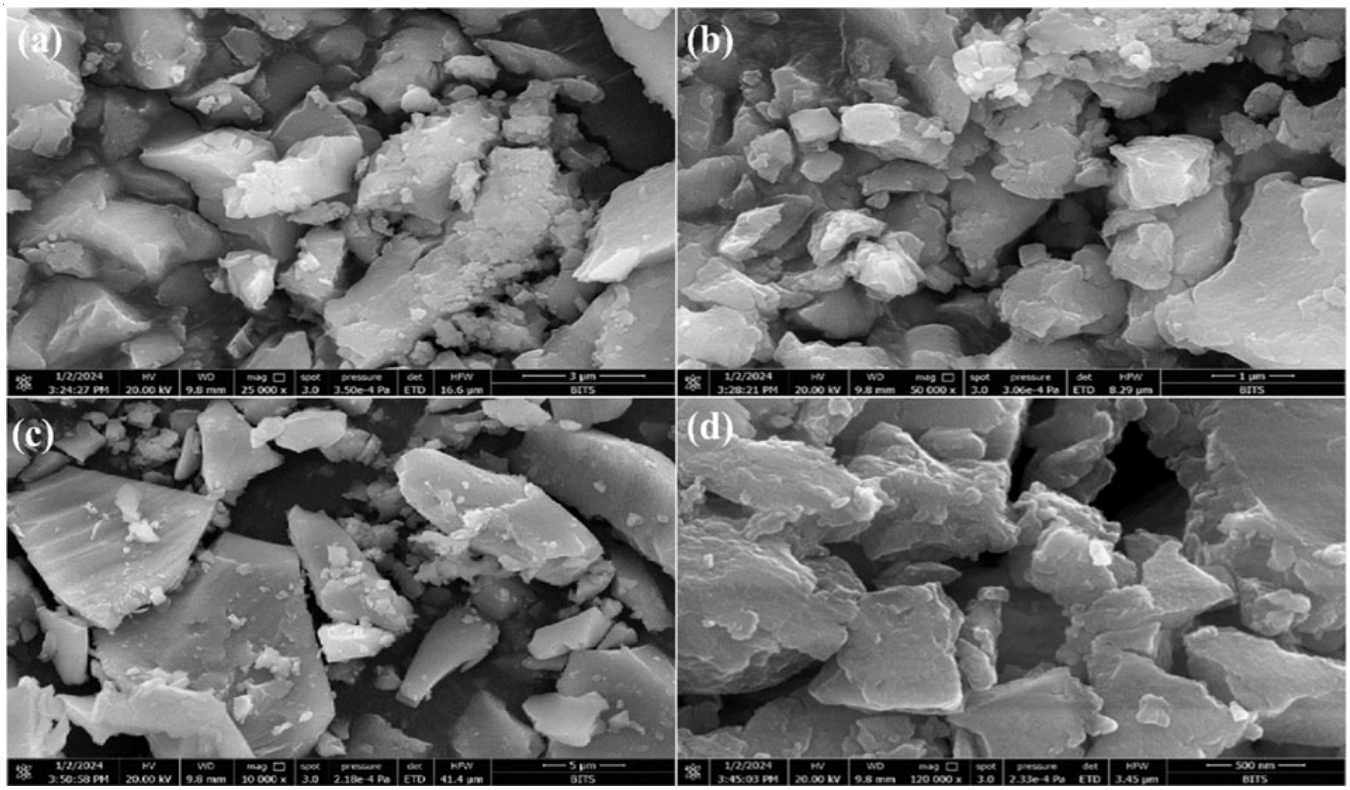

Fig. 2. FESEM images of synthesized BMOF

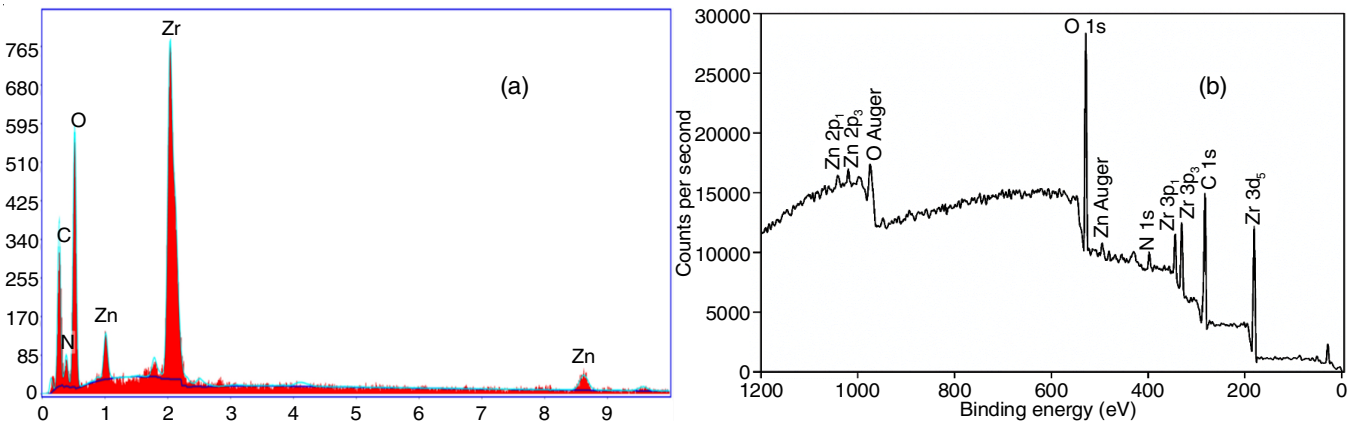

Fig. 3. (a) EDX and (b) XPS spectra of the synthesized BMOF

and zinc metals with 47% and 4% respectively. The spectra additionally reveal the presence carbon, nitrogen and oxygen elements with 20%, 4% and 25%, respectively. The particle size ranges from 0.300 to 30 µm based on the SEM images.

The XPS spectra displayed in Fig. 3b further demonstrates the Zr, Zn, O, N and C components present in BMOF. Zirconium sharp peaks of Zr $3p_3$, Zr $3p_1$ and Zr $3d_5$ are seen at 330, 343 and 181 eV respectively. Zn $2p_1$ can be seen at 1042 eV, Zn $2p_3$ peak is observed at 1021 eV and Zn Auger was shown at 496 eV. Sharp O 1s peak and short O Auger peak can be seen at 529 and 974 eV respectively. N 1s is shown at 397 eV and sharp C 1s peak is shown at 284 eV.

The SAED pattern and TEM images of the synthesized amorphous BMOF are shown in Fig. 4a-e. Particles of uneven shapes comprised the materials, which aggregated to form a mass on the TEM grid (Fig. 4a). Some particles are very porous and clustered in a spherical form, as seen in Fig. 4b. The deformed octahedral shape is observed in Fig. 4c, whereas the majority of the particles are clustered together and almost octahedral as seen in Fig. 4d. The absence of bright spots in the TEM's

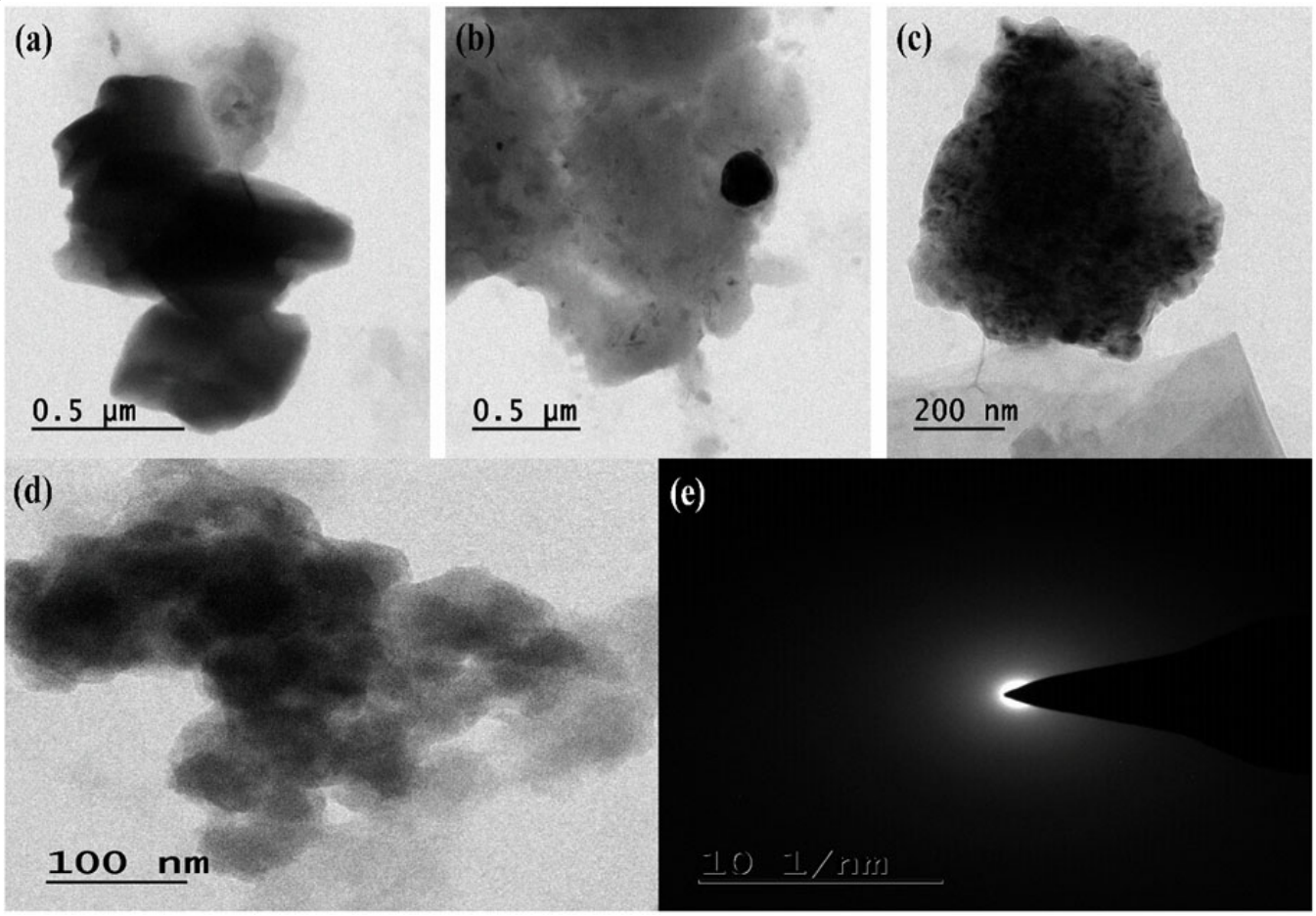

Fig. 4. (a-d) TEM images and (e) SAED pattern of amorphous BMOF

SAED pattern (Fig. 4e) gave additional proof that the generated material is amorphous or non-crystalline and this conclusion was in line with the powder XRD pattern of BMOF (Fig. 1b).

BET Studies: Using the N_2 gas adsorption/desorption isotherms from the Brunauer-Emmett-Teller (BET) gas-sorption experiments, the specific surface area and pore size distribution of the BMOF sample were determined. The N_2 adsorption–desorption curves of BMOF, a unique type-IV isotherm, are shown in Fig. 5 [21]. The BMOF's average pore diameter was measured to be 3.614 nm and its BET specific surface area was determined to be 316.49 m^2/g.

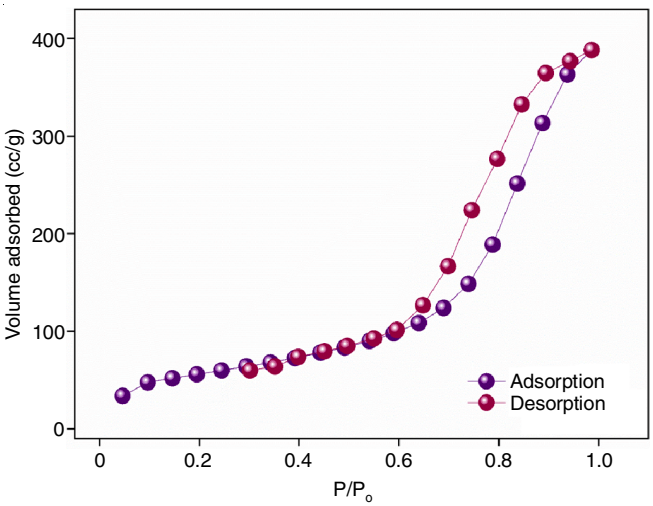

Fig. 5. N_2 adsorption/desorption isotherm of the synthesized BMOF

Fluorescence property: At room temperature, the BMOF fluorescence spectra were captured. After setting the excitation wavelength to 300 nm, the measurements of the emission spectra was captured. The BMOF has a maximum emission peak at 464 nm and provides fluorescence, while the EDTA ligand does not (Fig. 6). A suspension of 5 mg of BMOF sample was aged for 24 h after being sonicated for 40 min in 5 mL of double distilled water. Following a 24 h period, the suspension was transferred to a quartz cell with a width of 1 cm and the fluorescence spectra were obtained.

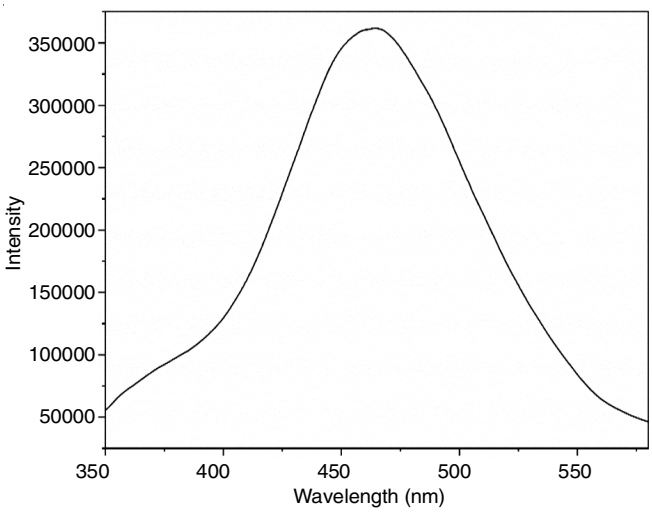

Fig. 6. Fluorescence spectrum of the synthesized BMOF

Sensing of antibiotics: The fluorescence responses of the BMOF were investigated towards the five common antibiotics *viz*. metronidazole (MDZ), ceftriaxone (CFT), ornidazole (ODZ), amikacin (AMK) and levofloxacin (LVF). After combining 5 mg BMOF sample with 5 mL of aqueous antibiotic solution (1×10^{-3} M), it was sonicated for approximately 40 min. The antibiotics MDZ, CFT and ODZ exhibit excellent quenching, as shown in Fig. 7, however the antibiotics LVF and AMK do not exhibit quenching due to a disparity in the wavelength of their maximum emission relative to the synthesized BMOF. Fig. 8 shows 98.79%, 98.63% and 98.14% quenching efficiency for CFT, MDZ and ODZ, respectively. The BMOF could potentially serve as a fluorescence sensor for ceftriaxone (CFT), metronidazole (MDZ) and ornidazole (ODZ) based on the aforementioned results. Further investigations into the BMOF's sensitivity to CFT, MDZ and ODZ was accomplished by the concentration-related experiment. As observed in Fig. 9a-c, the BMOF's emission intensity reduced dramatically from 1×10^{-6} M to 1×10^{-3} M as the antibiotic solutions concentration increased. Fig. 10 displays the quenching efficiency percentages for various CFT, MDZ and ODZ concentrations with the BMOF. The Stern-Volmer equation: $I_0/I = 1 + K_{sv} \times [M]$, can quantify the quenching efficiency of BMOF, where I_0 and I are the fluorescence intensity of BMOF aqueous solution in the absence and presence of CFT, MDZ and ODZ antibiotics, [M] is the molar concentration of analytes and K_{sv} (M^{-1}) is the quenching constant. The relation between fluorescence intensity and antibiotic concentration follows the Stern-Volmer (SV) equation at low concentrations; however, as concentration increases, the relationship deviates from linearity (Fig. 11). The equivalent K_{sv} values for CFT, MDZ and ODZ are 3.33×10^4 M^{-1}, 3.09×10^4 M^{-1} and 2.82×10^4 M^{-1}, respectively, based on the computed results. The formula for calculating the limit of detection (LOD) is $3\sigma/k_{sp}$ where σ and k_{sp} stand for the standard deviation and linear slope, respectively. The LOD of CFT, MDZ and ODZ is 4.9×10^{-7} M, 5.4×10^{-7} M and 6.05×10^{-7} M. These results suggest that the synthesized BMOF fluorescence sensor for CFT, MDZ and ODZ is a promising option. Moreover, the BMOF has shown effective recyclability for up to five cycles without affecting the PXRD pattern indicative of fluorescence quenching (Fig. 12).

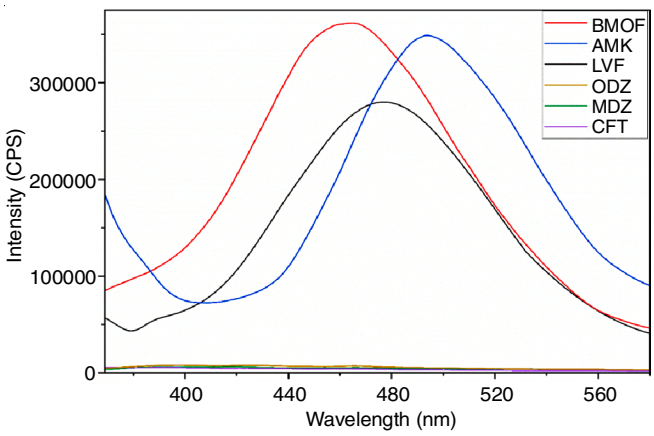

Fig. 7. Fluorescence spectra of the synthesized BMOF with all the selected antibiotics

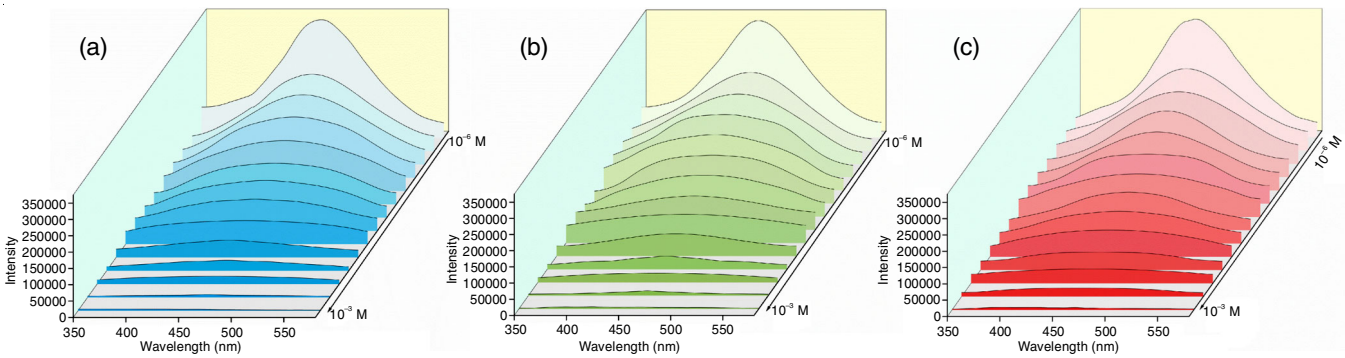

Fig. 9. Fluorescence spectra of BMOF with different concentrations of (a) ceftriaxone (CFT), (b) metronidazole (MDZ) and (c) ornidazole (ODZ)

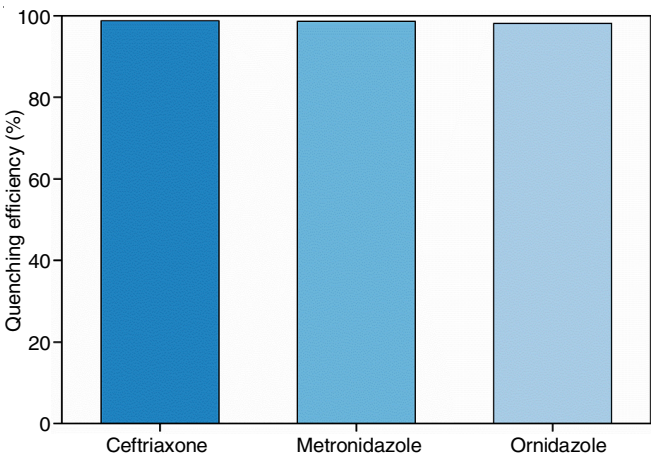

Fig. 8. Quenching efficiency percentages of BMOF with three different drugs

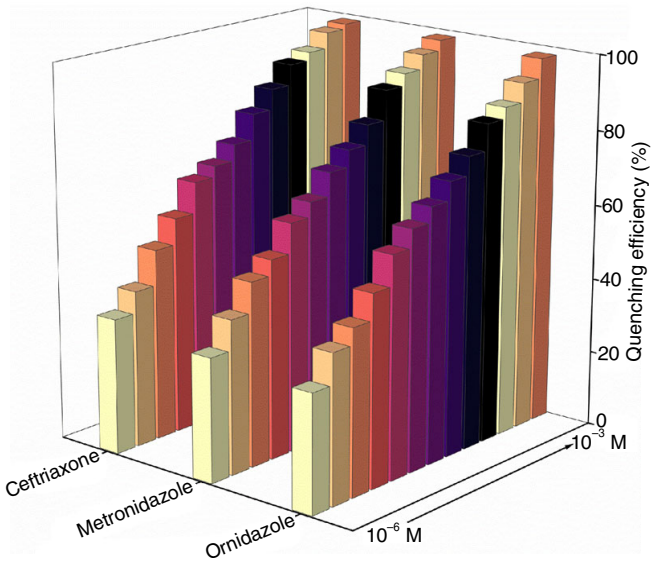

Fig. 10. Quenching efficiency percentages of BMOF with different concentrations of ceftriaxone (CFT), metronidazole (MDZ) and ornidazole (ODZ)

Fluorescence quenching mechanism: To understand the process of fluorescence quenching in BMOF, a plausible explanation for the detection of CFT and MDZ was investigated. In terms of structural analysis, the PXRD patterns of BMOF following the detection procedure matched the simulated pattern, showing that the skeleton had not broken properly. Thus, the

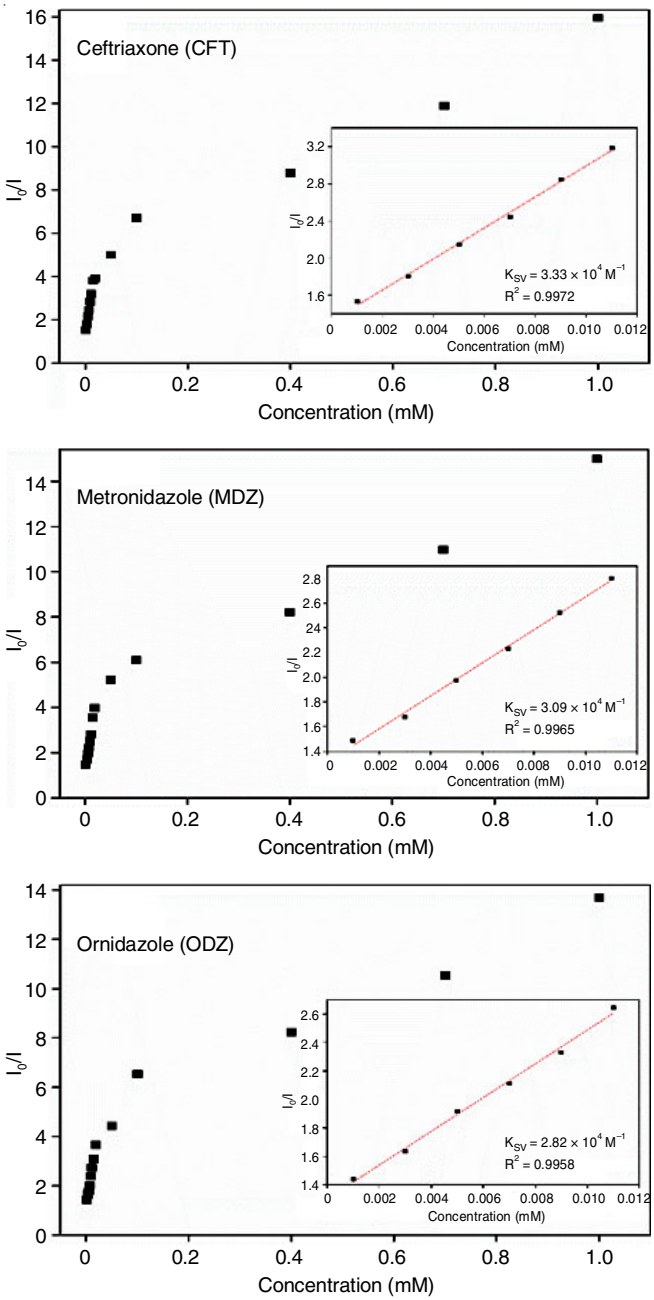

Fig. 11. Stern-Volmer plots of BMOF for sensing of ceftriaxone (CFT), metronidazole (MDZ) and ornidazole (ODZ) antibiotics. The inset shows linear fitting of the relative fluorescence intensity

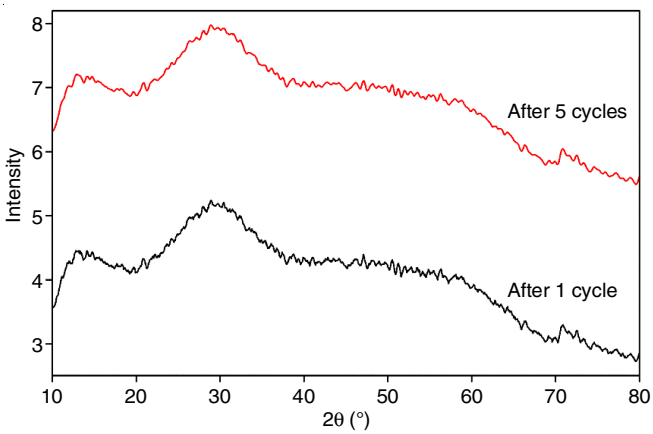

Fig. 12. XRD spectra after the recyclability of the prepared BMOF

fluorescence quenching was not caused by the breakdown of the structure. The photoinduced electron transfer (PET) between BMOF and antibiotics, in which the excited electrons of BMOF go to the lowest unoccupied molecular orbitals (LUMOs) of antibiotics, provides an explanation for the quenching process [22]. The resonance energy transfer is another possible quenching mechanism. In fact, the energy transfer that occurs during fluorescence quenching is evident from the non-linearity of the SV plots for antibiotics. Resonance energy can typically be transferred from BMOF to analyte in the presence of "inner filter effect" in which the added antibiotics absorb light energy at the BMOF excitation wavelength, leading to fluorescence quenching [23].

Conclusion

In conclusion, using zinc acetate, zirconium oxychloride and disodium salt of ethylenediamine tetra acetic acid, a novel fluorescence probe called Zr-Zn-EDTA bimetallic MOF (BMOF) was effectively prepared with outstanding water stability using a solvothermal approach. The fluorescence sensing studies of BMOF as a fluorescence sensor could swiftly, sensitively and selectively detect the antibiotics ceftriaxone (CFT), metronidazole (MDZ) and ornidazole (ODZ) with very low detection limits of 4.9×10^{-7} M, 5.4×10^{-7} M and 6.05×10^{-7} M, respectively and good five-cycle recyclable properties.

ACKNOWLEDGEMENTS

The authors gratefully acknowledges the Department of Chemistry, Andhra University for providing the research facilities and instrumentation assistance. The authors are also grateful to Advanced Analytical Laboratory of Andhra University, Indian Institute of Petroleum and Energy of Visakhapatnam, Indian Institute of Technology Hyderabad and the CSIF facility at Birla Institute of Technology & Science, Pilani and K K Birla Goa campus for preforming the thermogravimetric, P-XRD, X-ray photoelectron and FESEM-EDX spectroscopic analyses, respectively.

CONFLICT OF INTEREST

The authors declare that there is no conflict of interests regarding the publication of this article.

REFERENCES

1. M. Almasi, N. Kiraly, V. Zelenak, M. Vilkova and S. Bourrelly, *RSC Adv.*, **11**, 20137 (2021); https://doi.org/10.1039/D1RA02938J
2. T.D. Bennett and A.K. Cheetham, *Acc. Chem. Res.*, **47**, 1555 (2014); https://doi.org/10.1021/ar5000314
3. C. Orellana-Tavra, E.F. Baxter, T. Tian, T.D. Bennett, N.K.H. Slater, A.K. Cheetham and D. Fairen-Jimenez, *Chem. Commun.*, **51**, 13878 (2015); https://doi.org/10.1039/C5CC05237H
4. T.D. Bennett, P.J. Saines, D.A. Keen, J.C. Tan and A.K. Cheetham, *Chem. Eur. J.*, **19**, 7049 (2013); https://doi.org/10.1002/chem.201300216
5. F. Yang, W. Li and B. Tang, *J. Alloys Compd.*, **733**, 8 (2018); https://doi.org/10.1016/j.jallcom.2017.10.129
6. X. Zhang, H. Li, X. Lv, J. Xu, Y. Wang, C. He, N. Liu, Y. Yang and Y. Wang, *Chem. Eur. J.*, **24**, 8822 (2018); https://doi.org/10.1002/chem.201800773
7. Y. Jiao, J. Pei, D. Chen, C. Yan, Y. Hu, Q. Zhang and G. Chen, *J. Mater. Chem. A Mater. Energy Sustain.*, **5**, 1094 (2017); https://doi.org/10.1039/C6TA09805C
8. S. Mottola, A. Mancuso, O. Sacco, V. Vaiano and I. De Marco, *Catalysts*, **13**, 1173 (2023); https://doi.org/10.3390/catal13081173
9. M. Farré, L. Kantiani, M. Petrovic, S. Pérez and D. Barceló, *J. Chromatogr. A*, **1259**, 86 (2012); https://doi.org/10.1016/j.chroma.2012.07.024
10. M. González-Pleiter, S. Gonzalo, I. Rodea-Palomares, F. Leganés, R. Rosal, K. Boltes, E. Marco and F. Fernández-Piñas, *Water Res.*, **47**, 2050 (2013); https://doi.org/10.1016/j.watres.2013.01.020
11. R. Meffe and I. de Bustamante, *Sci. Total Environ.*, **481**, 280 (2014); https://doi.org/10.1016/j.scitotenv.2014.02.053
12. P. Karungamye, A. Rugaika, K. Mtei and R. Machunda, *J. Xenobiot.*, **12**, 223 (2022); https://doi.org/10.3390/jox12030017
13. T. Kokulnathan and S.M. Chen, *ACS Appl. Mater. Interfaces*, **11**, 7893 (2019); https://doi.org/10.1021/acsami.8b09204
14. Y. Zhang, L. Zhao, Y. Yang and P. Sun, *RSC Adv.*, **8**, 35062 (2018); https://doi.org/10.1039/C8RA04079F.
15. D. Li, S. He, Y. Deng, G. Ding, H. Ni and Y. Cao, *Bull. Environ. Contam. Toxicol.*, **93**, 47 (2014); https://doi.org/10.1007/s00128-014-1257-y
16. G.D. Wang, Y.Z. Li, W.J. Shi, B. Zhang, L. Hou and Y.Y. Wang, *Sens. Actuators B Chem.*, **331**, 129377 (2021); https://doi.org/10.1016/j.snb.2020.129377
17. X. Zhang, R. Yu, D. Wang, W. Li and Y. Zhang, *Front. Chem.*, **10**, 918941 (2022); https://doi.org/10.3389/fchem.2022.918941
18. J. Zhang, B. An, Z. Li, Y. Cao, Y. Dai, W. Wang, L. Zeng, W. Lin and C. Wang, *J. Am. Chem. Soc.*, **143**, 8829 (2021); https://doi.org/10.1021/jacs.1c03283
19. S. Momin, T. Mahmood, A. Ullah, A. Naeem and A. Khan, *Arab. J. Sci. Eng.*, **49**, 9269 (2024); https://doi.org/10.1007/s13369-023-08571-5
20. D.T. Sawyer and P.J. Paulsen, *J. Am. Chem. Soc.*, **81**, 816 (1959); https://doi.org/10.1021/ja01513a017
21. M.S. Mostafa, A.A. Bakr, Gh. Eshaq and M.M. Kamel, *Desalin. Water Treat.*, **56**, 239 (2015); https://doi.org/10.1080/19443994.2014.934725
22. J. Qin, B. Ma, X.F. Liu, H.L. Lu, X.Y. Dong, S.Q. Zang and H. Hou, *J. Mater. Chem. A Mater. Energy Sustain.*, **3**, 12690 (2015); https://doi.org/10.1039/C5TA00322A
23. Y. Ma, X. Yang, D. Shi, M. Niu and D. Schipper, *Inorg. Chem.*, **59**, 16809 (2020); https://doi.org/10.1021/acs.inorgchem.0c02567